Antiproliferative effects of palladium(II) complexes of 5-nitrosopyrimidines and interactions with the proteolytic regulatory enzymes of the renin–angiotensin system in tumoral bra...

ARTICLE *in* JOURNAL OF INORGANIC BIOCHEMISTRY · JUNE 2013

Impact Factor: 3.44 · DOI: 10.1016/j.jinorgbio.2013.06.005 · Source: PubMed

5 AUTHORS, INCLUDING:

José Manuel Martínez-Martos
Universidad de Jaén
142 PUBLICATIONS **824** CITATIONS
SEE PROFILE

María Jesús Ramírez-Expósito
Universidad de Jaén
131 PUBLICATIONS **734** CITATIONS
SEE PROFILE

Journal of Inorganic Biochemistry 126 (2013) 118–127

Contents lists available at SciVerse ScienceDirect

Journal of Inorganic Biochemistry

journal homepage: www.elsevier.com/locate/jinorgbio

Antiproliferative effects of palladium(II) complexes of 5-nitrosopyrimidines and interactions with the proteolytic regulatory enzymes of the renin–angiotensin system in tumoral brain cells

Nuria A. Illán-Cabeza [a], Antonio R. García-García [a], José M. Martínez-Martos [b], María J. Ramírez-Expósito [b], Miguel N. Moreno-Carretero [a,*]

[a] Departamento de Química Inorgánica y Orgánica, Universidad de Jaén, 23071 Jaén, Spain
[b] Departamento de Ciencias de la Salud, Universidad de Jaén, 23071 Jaén, Spain

ARTICLE INFO

Article history:
Received 20 March 2013
Received in revised form 10 June 2013
Accepted 10 June 2013
Available online 18 June 2013

Keywords:
Antiproliferative effect
Crystal structure
Palladium(II) complexes
Uracil
Violuric acid
Renin–angiotensin system

ABSTRACT

Seventeen new palladium(II) complexes of general formulaes $PdCl_2L$, $PdCl(LH_{-1})$(solvent) and $PdCl_2(PPh_3)_2L$ containing pyrimidine ligands derived from 6-amino-5-nitrosouracil and violuric acid have been prepared and characterized by elemental analysis, IR and NMR (^1H and ^{13}C) methods and, two of them, $PdCl(DANUH_{-1})(CH_3CN)]\cdot\frac{1}{2}H_2O$ and $[PdCl(2MeOANUH_{-1})(CH_3CN)]$ by X-ray single-crystal diffraction (DANU: 6-amino-1,3-dimethyl-5-nitrosouracil; 2MeOANU: 6-amino-2-methoxy-5-nitroso-3*H*-pyrimidin-4-one). The coordination environment around palladium is nearly square planar in the two compounds with different supramolecular arrangements. Crystallographic and spectral data are consistent with a bidentate coordination mode through N5 and O4 atoms when the ligands act in neutral form and N5 and N6 atoms in the monodeprotonated ones. The cytotoxicity of the complexes against human neuroblastoma (NB69) and human glioma (U373-MG) cell lines has been tested showing a considerable antiproliferative activity. Also, the study of the effects of palladium(II) complexes on the renin–angiotensin system (RAS) regulating proteolytic regulatory enzymes aminopeptidase A (APA), aminopeptidase N (APN) and insulin-regulated aminopeptidase (IRAP) shows a strong dependence on the compound tested and the tumoral cell type, also affecting different catalytic routes; the compounds affect in a different way the activities of enzymes of the RAS system, changing their functional roles as initiators of cell proliferation in tumors as autocrine/paracrine mediators.

1. Introduction

The great success of cisplatin in the clinical treatment of human malign tumor has motivated efforts to develop new antitumor agents with improved therapeutic properties [1–3]. The similarity between the coordination chemistry of platinum(II) and palladium(II) compounds supports the theory that palladium complexes can act successfully as antitumor drugs. Pd atom has a higher liability in ligand exchange (10^5-fold *vs* Pt) but the low antitumoral activity has been attributed to the rapid hydrolysis processes leading to dissociation of complex and formation of very reactive species unable to reach their biological targets. These problems can be solved by using bulky heterocyclic and chelating ligands such as aromatic N-containing compounds [4–8]. It is generally assumed that the antitumor properties of complexes strongly depend on the nature of the ligands and the metal coordination pattern. In this context, some palladium complexes with bidentate amine ligands have shown anticancer activity comparable or greater than cisplatin with fewer side effects if compared with other heavy metal anticancer compounds [9,10].

As the biological activity of a complex strongly depends on the nature of the ligands and on the metal coordination pattern, the recent research has been directed to synthesis and evaluation of complexes with biologically interesting ligands with the aim of widening the spectrum of complex activity [11,12]. Pyrimidine derivatives and compounds, in which the pyrimidine ring is part of a more complex system, are widely distributed in living organism and find application in biochemistry and clinical chemistry [13]. In particular, 5-nitrosopyrimidines have been used for analytical purpose and biological properties [14]. Some years ago, the antiproliferative behavior of a number of tricarbonylrhenium(I) compounds containing 6-amino-5-nitrosouracil derivatives was reported [15]; the evaluation against five human tumor cell lines suggested a modulator behavior of cell growth at low concentrations due to their estrogenic-like characteristics.

Now, our attention is also focused on the local tissue renin–angiotensin system (RAS) which has been involved in the development of several tumor types including mammary [16,17] and brain tumors [18]. In RAS system, several biologically active peptides and regulatory proteolytic enzymes are involved. Angiotensinogen (AGT) is converted

* Corresponding author. Tel.: +34 953 212738; fax: +34 953 211876.
E-mail address: mmoreno@ujaen.es (M.N. Moreno-Carretero).

0162-0134/$ – see front matter © 2013 Elsevier Inc. All rights reserved.
http://dx.doi.org/10.1016/j.jinorgbio.2013.06.005

Table 1
Crystal data and structure refinement for complexes [PdCl(DANUH$_{-1}$)(CH$_3$CN)]·½H$_2$O (**9**) and [PdCl(2MeOANUH$_{-1}$)(CH$_3$CN)] (**10**).

	[PdCl(DANUH$_{-1}$)(CH$_3$CN)]·½H$_2$O	[PdCl(2MeOANUH$_{-1}$)(CH$_3$CN)]
CCDC number	871269	871271
Empirical formula	$Pd_2C_{16}H_{20}N_{10}O_7Cl_2$[a]	$PdC_7H_8N_5O_3Cl$
Formula weight	748.12	352.05
Crystal system	Triclinic	Monoclinic
Space group	P −1	P 2$_1$/c
a (Å)	8.6817(6)	7.7776(5)
b (Å)	11.5495(6)	8.881(1)
c (Å)	13.8579(6)	8.4291(7)
α (°)	106.720(5)	90
β (°)	104.256(4)	116.260(7)
γ (°)	97.837(6)	90
Volume (Å^3)	1257.2(1)	1123.7(1)
Z	2	4
D_{calc} (g cm^{-3})	1.976	2.081
μ (mm^{-1})	1.701	1.893
F(000)	736	688
θ (°)	4.03–27.50	3.11–27.51
Limiting indices	$-11 \le h \le 11$	$-10 \le h \le 10$
	$-14 \le k \le 14$	$-24 \le k \le 24$
	$-17 \le l \le 17$	$-10 \le l \le 10$
Data/restrains/parameters	5746/0/374	2567/0/174
Goodness-of-fit on F^2	1.072	1.215
R_1/wR_2 [I > 2σ(I)]	0.0528/0.1218	0.0369/0.0898
R_1/wR_2 (all data)	0.0904/0.1502	0.0449/0.0960
Δρ (e Å^{-3})	1.369/−2.079	2.117/−0.926

([a]) Two independent molecules in the asymmetric unit.

into the inactive decapeptide angiotensin I (AngI) by the action of renin. Angiotensin-converting enzyme (ACE), the main effector of RAS, further converts AngI to AngII that acts on angiotensin II type 1 and 2 receptors (AT_1 and AT_2). Angiotensin II degradation begins with the action of aminopeptidase A (APA), which remove the N-terminal Asp to produce angiotensin III (AngIII), a less potent vasoconstrictor peptide than AngII [19,20]. AngIII is also produced from AngI through the production of des-Asp1-AngI, which is further converted to AngIII by the action of ACE. AngIII is further converted to angiotensin IV (AngIV) by aminopeptidase N (APN) [21]. Whereas AngI is considered inactive, AngII and AngIII are full agonists at the AT_1 and AT_2 receptors subtypes. Also, AngIV binds with low affinity at the AT_1 and AT_2, but with high affinity and specificity at the AT_4/IRAP receptor subtype. Furthermore, there is evidence that the AT_4 may be the insulin-regulated aminopeptidase (IRAP) [22,23].

In the present paper, the synthesis and structural characterization of several new mononuclear palladium(II) complexes with 5-nitrosopyrimidines as well as their antiproliferative activity and effects on the RAS-regulating proteolytic regulatory enzymes APA, APN and IRAP on the human tumor brain cell lines NB69 (neuroblastoma) and U373-MG (astroglioma) are reported.

2. Experimental

2.1. Instrumentation

C, H, N microanalyses were performed on a Thermofinnigan Flash 1112 Series elemental analyzer. Molar conductivities were measured on a Radiometer CMD2e apparatus (10^{-3} M dimethylformamide solutions). IR spectra were measured on a Bruker FT-IR Tensor-27 (4000–400 cm^{-1}, KBr pellets) and Vector-22 (600–220 cm^{-1}, polyethylene pellets) spectrophotometers. ^{1}H and ^{13}C NMR spectra were recorded using a Bruker Avance 400 apparatus (DMSO-d$_6$ solutions). Solid-state ^{13}C CP/TOSS (Cross-polaryzed total sideband suppression) NMR spectra were recorded with a Bruker-500 spectrometer.

2.2. Crystallography

Details of the crystallographic data collection and refinement parameters are given in Table 1. The measurements were performed on a Bruker-Nonius Kappa CCD diffractometer with graphite monochromated Mo-K$_\alpha$ (λ = 0.71073 Å) radiation. The temperature (120 K) was controlled employing an Oxford Cryosystem low-temperature device. Lorentz, polarization, and multiscan absorption corrections were applied with SADABS [24]. The structure was solved by direct methods and refined using SHELXL97 program [25] inside the WinGX package [26] employing full-matrix least-squares methods on F^2. All non-H atoms were refined anisotropically; all hydrogen atoms were placed in calculated positions following riding models except those corresponding to the 6-amino group and acetonitrile molecule, which were found in subsequent difference maps and isotropically refined. All calculations were carried out with PLATON [27] and graphics were drawn with MERCURY [28].

2.3. Synthesis of ligands and complexes

Commercial grade chemicals were used without further purification. The pyrimidine ligands were prepared by the methods described in our earlier reports [15,29]. The structure of the ligands is depicted in Fig. 1.

*2.3.1. $PdCl_2L$: $PdCl_2(ANU)\cdot H_2O$ (**1**), $PdCl_2(MANU)\cdot H_2O$ (**2**), $PdCl_2(DANU)\cdot ½CH_3OH$ (**3**), $PdCl_2(DANTU)\cdot ½CH_3OH$ (**4**), $PdCl_2(VIO)\cdot ½H_2O$ (**5**) and $PdCl_2(DVIO)\cdot H_2O$ (**6**)*

A suspension of the ligand (0.25 mmol) in hot MeOH (30 ml) was reacted with Na_2PdCl_4 (0.25 mmol). The mixture was stirred and heated for 9 h (50 °C). The solids were filtered, washed with EtOH and Et_2O and air dried. The complexes $PdCl_2(VIO)\cdot ½H_2O$ and $PdCl_2(DVIO)\cdot H_2O$ were obtained in CH_3CN in the same conditions. Several unsuccessful attempts to obtain XRD (X-Ray Diffraction) suitable single-crystals were made. $PdCl_2(ANU)\cdot H_2O$, Λ_M = 15.9 $\Omega^{-1}cm^2mol^{-1}$. ^{13}C NMR solid (δ ppm): 162.56 (C2), 175.03 (C4), 135.21 (C5), 150.31 (C6). $PdCl_2(MANU)\cdot H_2O$, Λ_M = 20.3 $\Omega^{-1}cm^2mol^{-1}$. ^{1}H NMR

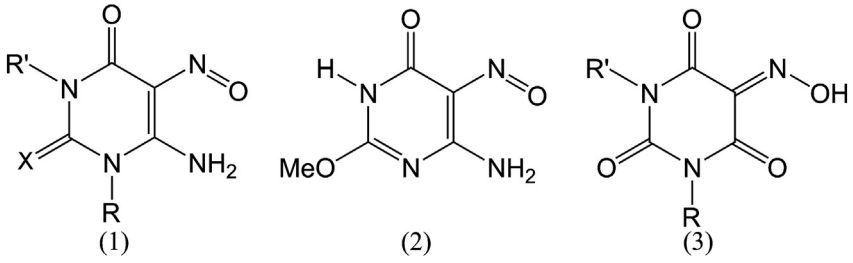

Fig. 1. More stable tautomeric structure and nomenclature of the ligands: (1) R = R′ = H, X = O, 6-amino-5-nitrosouracil (ANU, 6-amino-5-nitroso-1*H*-pyrimidin-2,4-dione); R = CH_3, R′ = H, X = O, 6-amino-1-methyl-5-nitrosouracil (MANU); R = R′ = CH_3, X = O, 6-amino-1,3-dimethyl-5-nitrosouracil (DANU); R = R′ = CH_3, X = S, 6-amino-1,3-dimethyl-5-nitroso-2-thiouracil (DANTU, 6-amino-1,3-dimethyl-5-nitroso-2-thioxo-2,3-dihydropyrimidin-4(1*H*)-one); (2) 6-amino-2-methoxy-5-nitroso-3*H*-pyrimidin-4-one (2MeOANU); (3) R = R′ = H, violuric acid (VIO, 5-hydroxyimino-pyrimidine-2,4,6(1*H*,3*H*,5*H*)-trione); R or R′ = CH_3, methylvioluric acid (MVIO); R = R′ = CH_3, dimethylvioluric acid (DVIO).

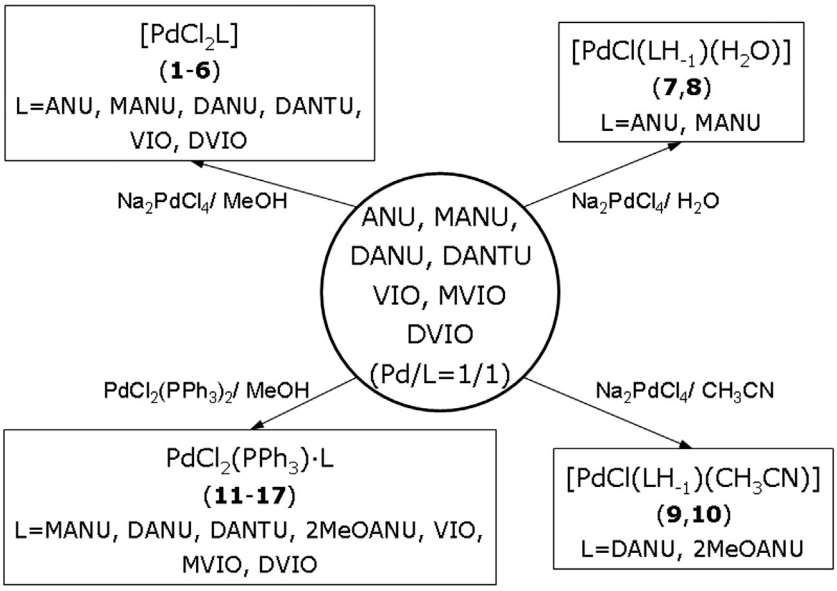

Fig. 2. Synthetic pathways for the title complexes.

data (δ, DMSO-d_6; Me_4Si): 3.28 (N1-CH_3), 8.30, 10.92 (C6-NH_2); ^{13}C NMR DMSO-d_6 (δ ppm): 28.59 (C1), 152.13 (C2), 148.42 (C6). ^{13}C NMR solid (δ ppm): 29.32 (C1), 155.34 (C2), 161.47 (C4), 142.43 (C5), 151.40 (C6). $PdCl_2$(DANU)·½CH_3OH, $\Lambda_M = 38.9\ \Omega^{-1}cm^2mol^{-1}$. ^1H NMR data (δ, DMSO-d_6; Me_4Si): 3.27 (N1-CH_3), 3.35 (N3-CH_3), 8.31, 12.88 (C6-NH_2); ^{13}C-NMR DMSO-d_6 (δ ppm): 28.58 (C1), 152.38 (C2), 29.33 (C3), 160.59 (C4), 139.42 (C5), 146.77 (C6); ^{13}C NMR solid (δ ppm): 31.17 (C1), 162.55 (C2), 33.85 (C3), 173.68 (C4), 134.93 (C5), 149.63 (C6). $PdCl_2$(DANTU)·½CH_3OH, $\Lambda_M = 3.4\ \Omega^{-1}cm^2mol^{-1}$. ^{13}C NMR solid (δ ppm): 36.52 (C1), 175.46 (C2), 38.30 (C3), 157.60 (C4), 142.06 (C5), 150.08 (C6). $PdCl_2$(VIO)·½H_2O, $\Lambda_M = 10.6\ \Omega^{-1}cm^2mol^{-1}$. ^1H NMR data (δ, DMSO-d_6; Me_4Si): 11.66 (N1-H), 10.81 (N3-H), 7.17 (C6-OH); ^{13}C NMR solid (δ ppm): 149.63 (C2), 174.57 (C4), 138.54 (C5), 154.33 (C6). $PdCl_2$(DVIO)·H_2O, $\Lambda_M = 60.5\ \Omega^{-1}cm^2mol^{-1}$. ^1H NMR data (δ, DMSO-d_6; Me_4Si): 3.23 (N1-CH_3), 3.29 (N3-CH_3), 7.15 (C6-OH); ^{13}C NMR DMSO-d_6 (δ ppm): 27.35 (C1), 28.13 (C3); ^{13}C NMR solid (δ ppm): 27.88 (C1), 150.08 (C2), 30.38 (C3), 175.46 (C4), 139.91 (C5), 154.53 (C6).

*2.3.2. PdCl(LH$_{-1}$)(solvent): PdCl(ANUH$_{-1}$)·1½H$_2$O (**7**), PdCl(MANUH$_{-1}$)·H$_2$O (**8**)*

The synthesis of these compounds was carried out by reacting 0.25 mmol of the ligand with 0.25 mmol of Na_2PdCl_4 in 30 mL H_2O. A suspension of the reaction product was obtained which was heated at 50 °C and stirred for about 3 h. The solids were filtered off and washed with EtOH and Et_2O. PdCl(ANUH$_{-1}$)·1½H_2O, $\Lambda_M = 1.6\ \Omega^{-1}cm^2mol^{-1}$. ^{13}C NMR solid (δ ppm): 174.43 (C2), 179.13 (C4), 135.09 (C5), 156.04 (C6). PdCl(MANUH$_{-1}$)·H_2O, $\Lambda_M = 2.6\ \Omega^{-1}cm^2mol^{-1}$. ^{13}C NMR DMSO-d_6 (δ ppm): 28.26 (C1), 158.00 (C2), 136.80 (C5), 148.04 (C6). ^{13}C NMR solid (δ ppm): 31.79 (C1), 160.24 (C2), 176.94 (C4), 134.87 (C5), 151.25 (C6).

*2.3.3. [PdCl(DANUH$_{-1}$)(CH$_3$CN)]·½H$_2$O (**9**), [PdCl(2MeOANUH$_{-1}$)(CH$_3$CN)] (**10**)*

The complexes were synthesized by reacting the corresponding organic precursor (0.25 mmol) and Na_2PdCl_4 (0.25 mmol) in CH_3CN. The reaction mixture was heated for 3 h. and, some days later, crystals suitable for X-ray diffraction were obtained. [PdCl(DANUH$_{-1}$)(CH_3CN)]·½H_2O, $\Lambda_M = 1.5\ \Omega^{-1}cm^2mol^{-1}$. ^1H NMR data (δ, DMSO-d_6; Me_4Si): 3.32 (N1-CH_3), 3.36 (N3-CH_3), 9.04 (C6-NH_2); ^{13}C NMR DMSO-d_6 (δ ppm): 26.71 (C1), 150.67 (C2), 28.87 (C3), 160.07 (C4), 137.22 (C5), 147.52 (C6); ^{13}C NMR solid (δ ppm): 152.24 (C2), 29.70 (C3), 162.07 (C4), 138.70 (C5), 149.40 (C6). [PdCl(2MeOANUH$_{-1}$)(CH_3CN)], $\Lambda_M = 5.4\ \Omega^{-1}cm^2mol^{-1}$. ^1H NMR data (δ, DMSO-d_6; Me_4Si): 3.92 (C2-OCH_3), 11.47 (N3-H), 9.50 (C6-NH_2); ^{13}C NMR DMSO-d_6 (δ ppm): 55.79 (−OCH_3), 158.41 (C2), 163.22 (C4), 153.37

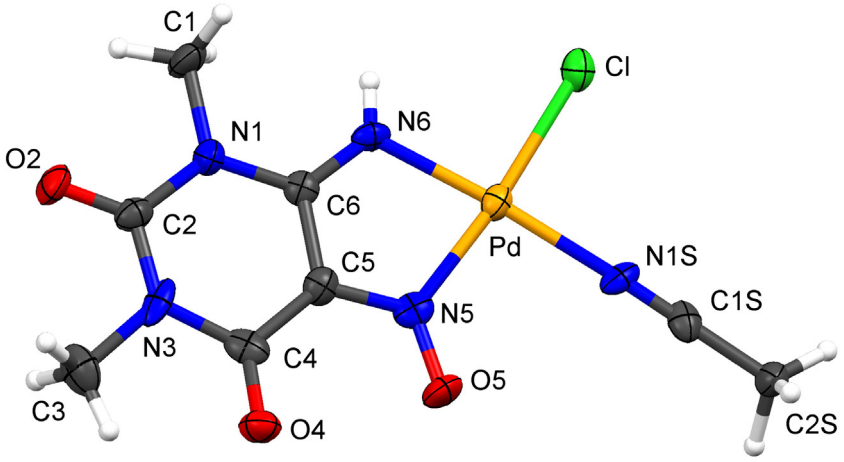

Fig. 3. ORTEP drawing (50% probability ellipsoids) and atom-labeling scheme for [PdCl(DANUH$_{-1}$)(CH_3CN)].

Table 2
Bond lengths (Å) and angles (°) around the palladium atom for complexes [PdCl(DANUH$_{-1}$)(CH3CN)]·½H$_2$O and [PdCl(2MeOANUH$_{-1}$)(CH$_3$CN)].

	[PdCl(DANUH$_{-1}$)(CH$_3$CN)]·½H$_2$O (two cryst. independent units in ARU)		[PdCl(2MeOANUH$_{-1}$)(CH$_3$CN)]
Pd-N5	2.006(5)	2.009(5)	2.001(3)
Pd-N6	1.992(6)	1.993(5)	1.963(3)
Pd-N1S	2.070(5)	2.037(5)	2.027(4)
Pd-Cl	2.331(2)	2.305(2)	2.292(1)
C2-O2	1.200(7)	1.205(8)	1.320(5)
O4-C4	1.220(8)	1.216(9)	1.233(5)
N5-C5	1.355(8)	1.341(8)	1.348(5)
N5-O5	1.232(6)	1.225(7)	1.249(4)
C6-N6	1.268(8)	1.275(8)	1.303(5)
N6-Pd-N5	80.2(2)	80.7(2)	81.4(1)
N6-Pd-N1S	175.8(2)	173.9(2)	178.1(1)
N5-Pd-N1S	95.6(2)	93.5(2)	97.1(1)
N6-Pd-Cl	94.0(2)	94.6(2)	92.2(1)
N5-Pd-Cl	174.2(2)	175.2(2)	173.3(1)
N1S-Pd-Cl	90.1(2)	91.3(1)	89.3(1)

(C6); ^{13}C NMR solid (δ ppm): 60.38 (−OCH$_3$), 161.72 (C2), 171.12 (C4), 138.66 (C5), 149.88 (C6).

*2.3.4. PdCl$_2$(PPh$_3$)$_2$L: PdCl$_2$(PPh$_3$)$_2$(MANU) (**11**), PdCl$_2$(PPh$_3$)$_2$(DANU) (**12**), PdCl$_2$(PPh$_3$)$_2$(DANTU)·CH$_3$OH (**13**), PdCl$_2$(PPh$_3$)$_2$(2MeOANU) (**14**), PdCl$_2$(PPh$_3$)$_2$(VIO) (**15**), PdCl$_2$(PPh$_3$)$_2$(MVIO) (**16**) and PdCl$_2$(PPh$_3$)$_2$(DVIO)·CH$_3$OH (**17**)*

A suspension of the organic ligand (0.25 mmol) in MeOH (30 ml) was mixed with *trans*-PdCl$_2$(PPh$_3$)$_2$ (0.25 mmol). The resulting solutions were heated for nine hours, and some days later, some solids precipitated which were filtered off and washed with EtOH and Et$_2$O. The compound PdCl$_2$(PPh$_3$)$_2$(VIO) was obtained with a similar procedure using stoichiometric KOH. In order to obtain XRD suitable single-crystals, several but unsuccessful recrystallizations were carried out. PdCl$_2$(PPh$_3$)$_2$(MANU), Λ_M = 5.2 Ω^{-1}cm^{2}mol^{-1}. ^{1}H NMR data (δ, DMSO-d$_6$; Me$_4$Si): 3.18 (N1-CH$_3$), 11.49 (N3-H), 9.08, 13.13 (C6-NH$_2$), 6.99–7.62 (m, 15H, C$_6$H$_5$); ^{13}C NMR DMSO-d$_6$ (δ ppm): 27.62 (C1), 148.79 (C2), 160.24 (C4), 138.73 (C5), 147.38 (C6), 128.70 (d, J_{CP} = 48 Hz, phenyl), 131.48 (phenyl); ^{13}C NMR solid (δ ppm): 28.95 (C1), 148.29 (C2), 158.54 (C4), 138.50 (C5), 146.07 (C6), 126.91–133.59 (broad signal, PPh$_3$). PdCl$_2$(PPh$_3$)$_2$(DANU), Λ_M = 16.7 Ω^{-1}cm^{2}mol^{-1}. ^{1}H NMR data (δ, DMSO-d$_6$; Me$_4$Si): 3.25 (N1-CH$_3$), 3.27 (N3-CH$_3$), 9.10, 12.98 (C6-NH$_2$), 6.65–7.87 (m, 15H, C$_6$H$_5$); ^{13}C NMR DMSO-d$_6$ (δ ppm): 27.59 (C1), 30.40 (C3), 128.71 (d, J_{CP} = 48 Hz, phenyl), 131.43 (d, J_{CP} = 40 Hz, phenyl), 131.98 (d, J_{CP} = 12 Hz, phenyl); ^{13}C NMR solid (δ ppm): 27.30 (C1), 150.29 (C2), 29.87 (C3), 160.56 (C4), 139.05 (C5), 148.04 (C6), 126.85–132.62 (broad signal, PPh$_3$). PdCl$_2$(PPh$_3$)$_2$(DANTU)·CH$_3$OH, Λ_M = 17.9 Ω^{-1}cm^{2}mol^{-1}. ^{1}H NMR data (δ, DMSO-d$_6$; Me$_4$Si): 3.77 (N1-CH$_3$), 3.75 (N3-CH$_3$), 8.81, 12.80 (C6-NH$_2$), 6.93–8.81 (m, 15H, C$_6$H$_5$); ^{13}C NMR DMSO-d$_6$ (δ ppm): 35.32 (C3), 128.70 (d, J_{CP} = 44 Hz, phenyl), 131.43 (d, J_{CP} = 40 Hz, phenyl), 131.98 (d, J_{CP} = 12 Hz, phenyl); ^{13}C NMR solid (δ ppm): 37.85 (C1), 175.01 (C2), 35.18 (C3), 156.76 (C4), 141.61 (C5), 150.08 (C6), 127.36–133.15 (broad signal, PPh$_3$). PdCl$_2$(PPh$_3$)$_2$(MeOANU), Λ_M = 10.4 Ω^{-1}cm^{2}mol^{-1}. ^{1}H NMR data (δ, DMSO-d$_6$; Me$_4$Si): 3.96 (C2-CH$_3$),11.36 (N3-H), 9.12, 12.32 (C6-NH$_2$), 6.42–7.85 (m, 15H, C$_6$H$_5$); ^{13}C NMR DMSO-d$_6$ (δ ppm): 55.56 (−OCH$_3$), 128.71 (d, J_{CP} = 48 Hz, phenyl), 131.43 (d, J_{CP} = 40 Hz, phenyl), 131.99 (d, J_{CP} = 8 Hz, phenyl); ^{13}C NMR solid (δ ppm): 58.34 (−OCH$_3$), 157.88 (C2), 161.69 (C4), 142.85 (C5), 149.13 (C6), 126.91–130.03 (broad signal, PPh$_3$). PdCl$_2$(PPh$_3$)$_2$(VIO), Λ_M = 15.1 Ω^{-1}cm^{2}mol^{-1}. ^{1}H NMR data (δ, DMSO-d$_6$; Me$_4$Si): 10.74 (N1-H), 10.06 (N3-H), 7.64 (C6-OH), 7.22–7.53 (m, 15H, C$_6$H$_5$); ^{13}C NMR DMSO-d$_6$ (δ ppm): 128.72 (d, J_{CP} = 40 Hz, phenyl), 130.92 (d, J_{CP} = 20 Hz, phenyl), 133.92 (d, J_{CP} = 20 Hz, phenyl); ^{13}C NMR solid (δ ppm): 147.85 (C2), 164.33 (C4), 140.28 (C5), 150.52 (C6), 129.14–131.82 (broad signal, PPh$_3$). PdCl$_2$(PPh$_3$)$_2$(MVIO), Λ_M = 16.3 Ω^{-1}cm^{2}mol^{-1}. ^{1}H NMR data (δ, DMSO-d$_6$; Me$_4$Si): 3.12 (N1-CH$_3$), 11.63 (N3-H), 14.59 (N5-OH), 7.06–7.76 (m, 15H, C$_6$H$_5$); ^{13}C NMR DMSO-d$_6$ (δ ppm): 27.84 (C1), 128.71 (d, J_{CP} = 48 Hz, phenyl), 131.43 (d, J_{CP} = 40 Hz, phenyl), 131.98 (d, J_{CP} = 12 Hz, phenyl); ^{13}C NMR solid (δ ppm): 28.06 (C1), 151.86 (C2), 158.54 (C4), 140.28 (C5), 154.08 (C6), 128.25–133.60 (broad

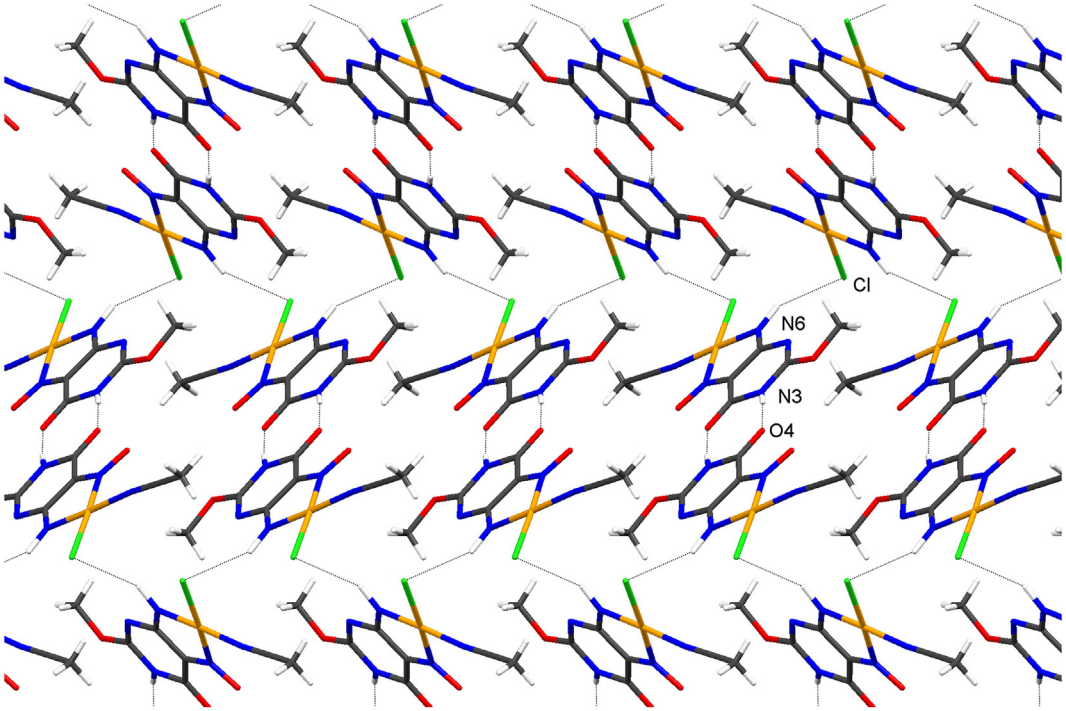

Fig. 4. Crystal packing diagram of [PdCl(2MeOANUH$_{-1}$)(CH$_3$CN)] from the *a* direction showing a H-bonded folded sheet. H bond parameters (D···A, ∠D-H···A) are as follows: N3-H···O4 (1 − x, -y, 1 − z), 2.863(5) Å, 173(6)°; N6-H···Cl (−1 + x, ½ − y, ½ + z), 3.558(3) Å, 153(4)°.

signal, PPh_3). $PdCl_2(PPh_3)_2(DVIO)\cdot CH_3OH$, $\Lambda_M = 4.4\ \Omega^{-1}cm^2mol^{-1}$. ^1H NMR data (δ, DMSO-d_6; Me_4Si): 3.13 (N1-CH_3), 3.19 (N3-CH_3), 14.70 (N5-OH), 6.96–7.65 (m, 15H, C_6H_5); ^{13}C NMR DMSO-d_6 (δ ppm): 27.52 (C1), 150.61 (C2), 28.20 (C3), 158.18 (C4), 135.65 (C5), 153.54 (C6), 128.71 (d, $J_{CP} = 48$ Hz, phenyl), 131.43 (d, $J_{CP} = 40$ Hz, phenyl), 131.98 (d, $J_{CP} = 8$ Hz, phenyl); ^{13}C NMR solid (δ ppm): 27.61 (C1), 150.52 (C2), 160.76 (C4), 139.38 (C5), 154.08 (C6), 127.36–133.03 (broad signal, PPh_3).

A brief description of the synthetic pathway for the isolation of palladium(II) complexes is depicted in Fig. 2. Elemental analyses (C, H, N, S) are in accordance with the proposed formulas. In the Supplementary material, detailed analytical and IR data are available.

2.4. Cell culture

Human neuroblastoma NB69 and astroglioma U373-MG cells were grown in 5% fetal bovine serum (FBS)-supplemented DMEM (Dulbecco's modified eagle's medium) medium without antibiotics. Cells were incubated at 37 °C in a modified atmosphere of 5% CO_2/95% air until reaching confluence. Freedom from mycoplasma contamination was checked regularly by testing with Hoechst 33528.

2.5. Colorimetric cytotoxic assay

To set up the colorimetric cytotoxic assay (CCA) cells were trypsinized from monolayer and diluted to 4×10^4 cells/mL. Cells were in exponential phase of growth during the whole experiment. Aliquots of 1 mL of cells were pipetted into wells of 24-well tissue culture plates (Nunc) and the plates were incubated for 24 h. The palladium(II) complexes were then added in triplicate to the wells in a volume of 1 mL per well at a range of concentrations (1–10 μM), each dose being used at least four replicate wells. After 3 days of incubation, the mediums were removed and the cultures were washed with PBS (phosphate buffered saline) prior to fixation with 10% trichloroacetic acid (TCA) (4 °C) for 30 min and then washed with tap water to remove TCA. Plates were air dried and then stored until use. TCA-fixed cells were stained for 20 min with 0.4% (w/v) sulforhodamine B (SRB) dissolved in 1% acetic acid. At the end of staining period, SRB was removed and cultures were rinsed with 1% acetic acid to remove unbound dye. The cultures were air dried and bound dye was solubilized with 10 mM Tris base (pH 10.5). Optical density (OD) was read in a Tecan Genios Plus plate reader at 492 nm. The photometer response was linear with dye concentration and it was proportional to cell numbers counted in parallel with an automatic cell counter (TC-10, Bio-Rad).

2.6. Aminopeptidase A activity assay

APA activity was analyzed in whole cells, using glutamyl-β-naphthylamide (GluNNap) as substrate. After removal of the culture medium, the cells were incubated by triplicate for 30 min at 37 °C with 100 μL of the assay medium containing the palladium(II) compounds at a range of concentrations (1–5 μM), 100 μM of GluNNap and 0.65 mM dithiothreitol (DTT), in artificial cerebrospinal fluid (NaCl 116 mM, KCl 5.4 mM, $MgCl_2$ 0.9 mM, $CaCl_2$ 1.8 mM, $NaHCO_3$ 25 mM, glucose 10 mM) pH 7.2.

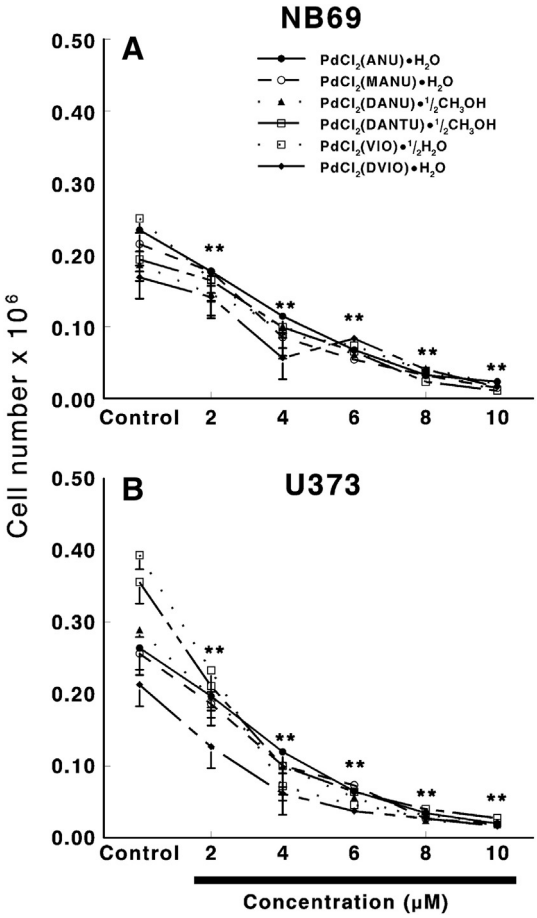

Fig. 5. Growth inhibition curves for human NB69 neuroblastoma (A) and U373-MG glioma (B) cell lines, measured by the colorimetric cytotoxicity assay (CCA) after the treatment with complexes $PdCl_2L$. Results are expressed as mean ± SD; n = 4; **P < 0.05).

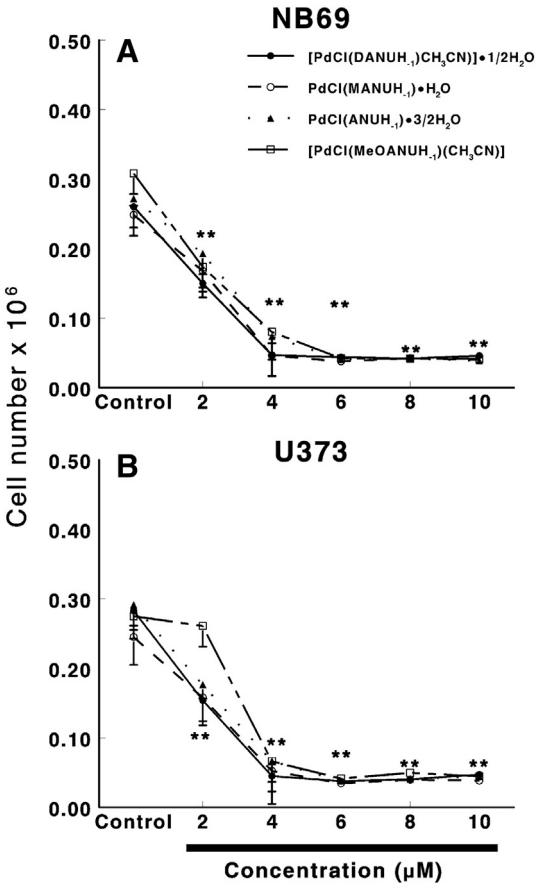

Fig. 6. Growth inhibition curves for human NB69 neuroblastoma (A) and U373-MG glioma (B) cell lines, measured by the colorimetric cytotoxicity assay (CCA) after the treatment with complexes $PdCl(LH_{-1})$(solvent). Results are expressed as mean ± SD; n = 4; **P < 0.05).

2.7. Aminopeptidase N assay

APN was also measured fluorometrically in whole cells using alanyl-β-naphthylamide (AlaNNap) as substrate. After removal of the culture medium, the cells were incubated by triplicate for 30 min at 37 °C with 100 μL of the substrate solution containing the complexes at a range of concentrations (1–5 μM), 100 μM of AlaNNap and 0.65 mM DTT in artificial cerebrospinal fluid (NaCl 116 mM, KCl 5.4 mM, $MgCl_2$ 0.9 mM, $CaCl_2$ 1.8 mM, $NaHCO_3$ 25 mM, glucose 10 mM) pH 7.2.

2.8. Insulin-regulated aminopeptidase activity assay

IRAP was measured fluorometrically in whole cells using leucyl-β-naphthylamide (LeuNNap) as substrate. After removal of the culture medium, the cells were incubated by triplicate for 30 min at 37 °C with 100 μL of the substrate solution containing the palladium(II) complexes at a range of concentrations (1–5 μM), 100 μM of LeuNNap and 0.65 mM DTT in artificial cerebrospinal fluid (NaCl 116 mM, KCl 5.4 mM, $MgCl_2$ 0.9 mM, $CaCl_2$ 1.8 mM, $NaHCO_3$ 25 mM, glucose 10 mM) pH 7.2.

The reactions were stopped by addition of 100 μL of acetate buffer 0.1 M (pH 4.2) and the amount of ß-naphthylamine released as the result of the enzymatic activities was measured fluorometrically at 412 nm emission wavelength with and excitation wavelength of 345 nm. Specific enzyme activities were expressed as picomoles of the corresponding aminoacyl-β-naphthylamide hydrolyzed per min per 10^6 cells, by using a standard curve prepared with the latter compound under corresponding assay conditions.

2.9. Statistics

We used one-way analysis of variance (ANOVA) to analyze differences between groups. Post-hoc comparisons were made using Newman–Keuls test P-values below 0.05 were considered significant.

3. Results and discussion

The molar conductivity values were measured in DMF solution. All the complexes show a non-electrolite nature except $PdCl_2(DVIO)\cdot H_2O$ [30]. This compound seems to be a 1:1 electrolyte but the IR spectrum (far-infrared region) shows two bands around 330 cm^{-1} which suggests terminal chlorine atoms in a *cis* arrangement, so the high conductivity value can be due to solvolisis processes.

3.1. Crystallographic studies on $[PdCl(DANUH_{-1})(CH_3CN)]\cdot ½H_2O$ (**9**) and $[PdCl(2MeOANUH_{-1})(CH_3CN)]$ (**10**)

A view of the molecular unit of the complex $[PdCl(DANUH_{-1})(CH_3CN)]$ (**9**) is shown in the Fig. 3. The coordination behavior of the pyrimidine ligand is similar in both compounds **9** and **10**. Selected interatomic distances and angles useful to describe the metal coordination spheres are given in Table 2.

In both compounds, the metal is square-planar four-coordinated by a chloride ion, the nitrogen atom from a acetonitrile molecule and a (N5,N6)-5-nitrosopyrimidine bidentate ligand. The *bite* angle formed by N5-Pd-N6 is significantly narrowed from the expected octahedral 90° value to 80°. Both pyrimidine ligands are virtually planar and coplanar with the chelate ring, the dihedral angle described being 3.5(3)° (**9**) and 1.3(3)° (**10**). Upon coordination, some changes in the bond lengths of the organic precursors DANU and 2MeOANU to palladium(II) are induced. The C6-N6 distances are shorter than the ones in the free ligands [31,32] (between 0.010 and 0.030 Å) showing an increased imino character, whereas the nitroso character of the 5-NO group is enhanced by means of shorter N5-O5 and longer C5-N5 distances, this behavior being typical of monodeprotonated 6-amino-5-nitrosopyrimidine ligands [33,34].

The crystal structure $[PdCl(DANUH_{-1})(CH_3CN)]\cdot ½H_2O$ consists in H-bond chains parallel to *a* direction between the deprotonated 6-amino group and water molecules. Each chain consists of four superimposed molecular units following the *c* direction; H bonds parameters (D···A, ∠D-H···A) are as follows: N6-H···O1w, 2.88(1) Å, 136(5)°; N6′-H···O2w (1 + x, y, z), 2.83(1) Å, 172(10)°; N6′-H···O1w (1 − x, 1 − y, 1 − z), 2.87(1) Å, 126(7)°; N6′-H···O2w (1 − x, 1 − y, 2 − z), 3.10(1) Å, 151(8)°. In addition to H-bonds, the analysis of the structure with PLATON [27] shows the existence of three different Van der Waals' interactions assembling the chains themselves and to each other [35]; thus, there are (a) π-π stacking between chelate rings (1 − x, 1 − y, 1 − z; Cg···Cg, 3.291(3) Å; slippage, 0.104 Å) and uracil rings (1 − x, 1 − y, 2-z; Cg···Cg, 3.327(3) Å; slippage, 0.444 Å), (b) Pd···π ring interactions with Pd···Cg and β *ca.* 3.3–3.4 Å and 7–9°, respectively, and (c) Y-X···π ring interactions between Pd1-Cl···py (1 − x, 1 − y, 1 − z) (Cl···Cg, 3.547(3) Å, Pd-Cl···Cg, 88.37(7)°) and Pd2-Cl···py (1 − x, 1 − y, 1 − z) (Cl···Cg, 3.635(3) Å, Pd-Cl···Cg, 86.40(7)°).

The molecular units in $[PdCl(2MeOANUH_{-1})(CH_3CN)]$ are H-bond arranged as folded planes growing along *b* and *c* axes (Fig. 4), with the *quasi*-coplanar pyrimidine/chelate rings roughly parallel to the [−1 0 1] direction. These planes are pilled up by means of Y-X · · · π ring Van der Waals' interactions between Pd-Cl···py (1 + x, y, z) (Cl···Cg, 3.728(2) Å, Pd-Cl···Cg, 97.11(4)°), C4-O4···chelate (2 − x, -y, 1 − z) (O4···Cg, 3.416(4) Å, C4-O4···Cg, 100.8(3)°) and N5-O5···py (2 − x, -y, 1 − z) (O5···Cg, 3.298(4) Å, N5-O5···Cg, 107.8(2)°).

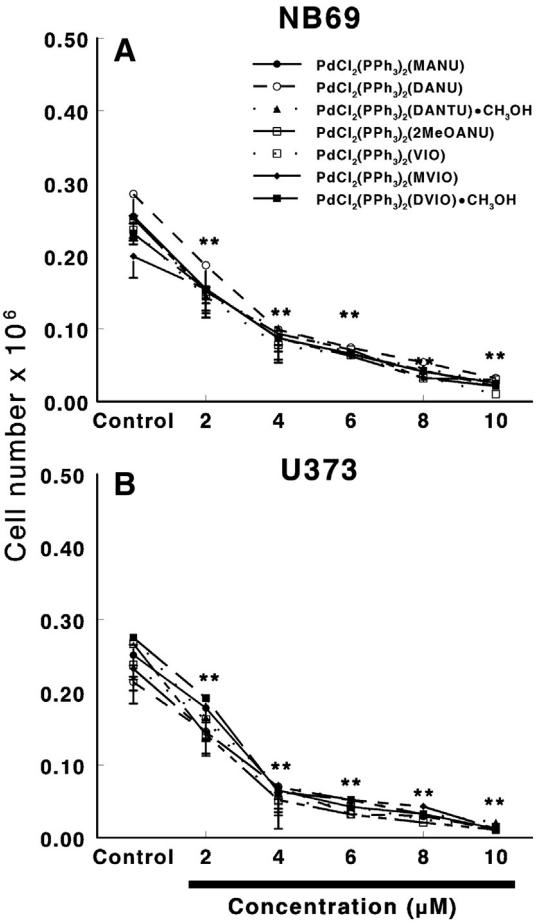

Fig. 7. Growth inhibition curves for human NB69 neuroblastoma (A) and U373-MG glioma (B) cell lines, measured by the colorimetric cytotoxicity assay (CCA) after the treatment with complexes $PdCl_2(PPh_3)_2L$. Results are expressed as mean ± SD; n = 4; **P < 0.05).

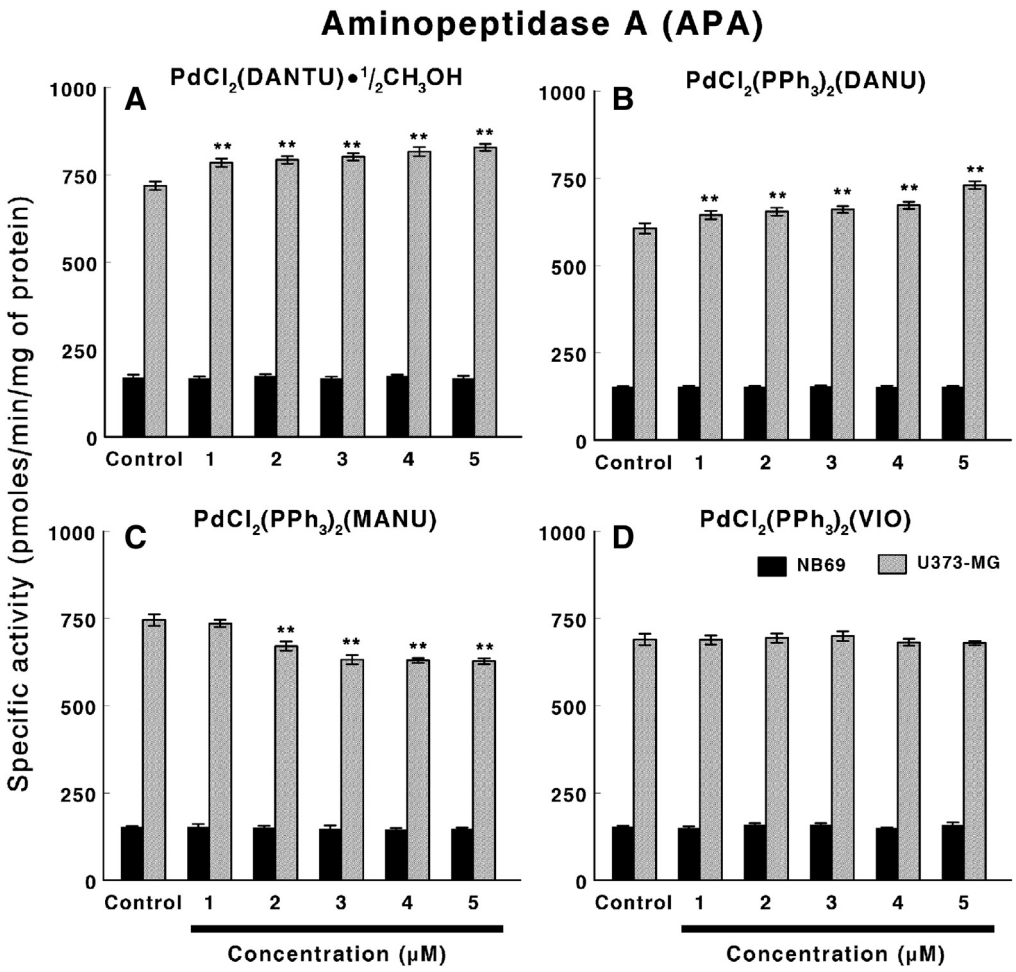

Fig. 8. Aminopeptidase A (APA) specific activity in human NB69 neuroblastoma and U373-MG glioma cell lines after the treatment with the palladium complexes **4** (A), **12** (B), **11** (C) and **15** (D). Results are expressed in pmol/min/mg of protein (Mean ± SEM; $^{**}P < 0.01$; n = 4).

3.2. Spectral studies

Tentative assignments for the more significative bands of infrared spectra of metal complexes have been made by comparison with the ligands ones [15,29] and literature data [36]. In the infrared spectra of the complexes with the deprotonated 6-amino-5-nitrosopyrimidine ligands, there are significant changes in the ν(N–H) bands, as consequence of both coordination and deprotonation processes, the most remarkable being the appearance of a very sharp and strong band, at around 3300–3400 cm^{-1}, assigned to the ν(N–H) mode of an imino group. In general, ν(C═O) carbonyl bands appear at higher wavenumber in the infrared spectra (*ca.* 1740 and 1670 cm^{-1}) of the complexes $PdCl_2L$ (**1**–**6**) and $PdCl_2(PPh_3)_2L$ (**11**–**17**) (neutral pyrimidine ligands), than in those corresponding to complexes $PdCl(LH_{-1})$ (**7**–**10**) (N6-monodeprotonated pyrimidine ligand) (*ca.* 1710 and 1640 cm^{-1}); this fact strongly indicates that, on deprotonation, a growing presence of enolyzed forms of the pyrimidine ligands takes place.

Upon complexation, the organic ligand in the palladium(II) complexes with violuric acids shows a tautomeric change from the oxime metal-free form to the coordinated-nitroso one [37], in both deprotonated and neutral forms, as evidenced by the appearance of the ν(N═O) band (*ca.* 1500 cm^{-1}) and the disappearance of the ν(N–O) band (*ca.* 1000 cm^{-1}) [38–40]. Also, the bands assignable to C–O stretching vibrations are also shifted as consequence of the possible coordination of the carbonyl oxygen O4. The complexes with general formula $PdCl_2(PPh_3)_2L$ show bands indicating the presence of PPh_3 (*ca.* 3050, 1435, 1090 and 707 cm^{-1}).

In the far-infrared region, bands between 360–310 cm^{-1}, assignable to ν(Pd-Cl) vibrations, can be observed [41,42]. Two bands for $PdCl_2L$ complexes (**1**–**6**) indicate terminal chlorine atoms in *cis* arrangement, this fact being in accordance with a mononuclear structure with the organic ligand in bidentate form; also, the presence of a unique band for this vibration mode in $PdCl(LH_{-1})$(solvent) compounds (**7**–**10**) confirms the mononuclear structure found from XRD measurements whereas, for compounds $PdCl_2(PPh_3)_2L$ (**11**–**17**), only the presence of *trans*-Pd-Cl bonds can be affirmed.

It has not been possible to record the NMR spectra of some Pd(II) compounds due to their low solubility in DMSO-d_6. In other cases, the NMR spectra display signals at the same values of chemical shift found for free ligands, clearly indicating that these compounds undergo strong solvolisis. A strong intramolecular H-bond in the 6-amino-5-nitrosouracil derivatives is established between the oxygen atom from the 5-nitroso group and one hydrogen atom from the 6-amino group which justifies the appearance of two signals in ^{1}H NMR spectra at around 12 and 10 ppm, the proton involved in the H-bond being downfield shifted. The violuric ligands in the palladium(II) complexes are found in the nitroso-enol tautomeric form regardless the deprotonation state. In the ^{1}H NMR spectrum of the complexed neutral violuric ligands is observed a signal at around 7.15 ppm which corresponds to the hydroxyl group of nitroso-enol tautomeric form.

On comparing the ^{13}C NMR spectra of complexes in solid state with those of free 6-amino-5-nitrosouracil derivatives, a downfield shift of the signal of the C4 atom (~12–18 ppm) can be observed suggesting the charge redistribution after the coordination process. The signal of C5 atom is upfield shifted and changes in the C2 and

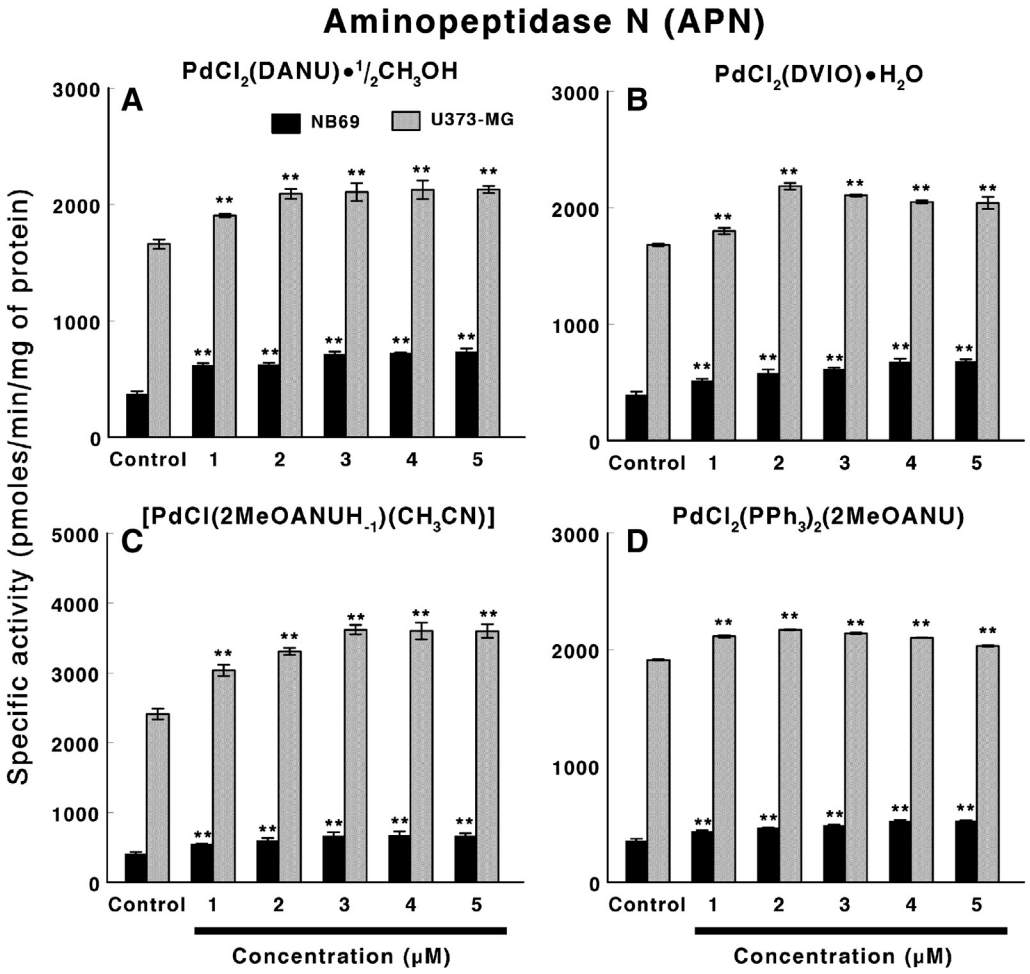

Fig. 9. Aminopeptidase N (APN) specific activity in human NB69 neuroblastoma and U373-MG glioma cell lines after the treatment with the palladium complexes **3** (A), **6** (B), **10** (C) and **14** (D). Results are expressed in pmol/min/mg of protein (Mean ± SEM; $^{**}P < 0.01$; n = 4).

C6 signals are also observed. When the ligands act in deprotonated form, C5 is deshielded because of the coordination of the nitroso group to metal atom and C6 signal changes as consequence both deprotonation and coordination processes. The coordination and the change in tautomerism in palladium(II) complexes with violuric acids induce a significant deshielding of C4 and C5 signals.

In view of the obtained data, mononuclear square-planar structures *cis*-[$PdCl_2$(N5,O4-L)] (complexes **1**–**6**) and *cis*-[PdCl(N5,N6-LH_{-1})(solvent)] (complexes **7**–**10**) may be proposed. For the complexes **11**–**17**, some singular features can be reported, but the only spectral data do not allow us to propose any certain structure; perhaps, the existence of an adduct between *trans*-$PdCl_2(PPh_3)_2$ and the pyrimidine moiety could be suggested, with relatively weak interactions between $PdCl_2P_2$ centers and pyrimidine ligands. Further XRD studies would be needed to know how the bond between them is established.

3.3. Biological studies

In order to assess the antiproliferative potential of the complexes, cytotoxicity assays were performed *in vitro* using two human cell lines. Growth inhibition curves for NB69 human neuroblastoma and U373-MG human glioma cells measured by the colorimetric cytotoxic assay after the treatment with the different complexes are shown in Figs. 5, 6 and 7. All the palladium(II) complexes tested displayed similar cytotoxic effects in both tumoral cell lines used. They showed a significant inhibition of cell growth on increasing the concentration. The complexation of palladium to the different pyrimidine ligands has a non-specific effect inducing cell death.

More interesting are the effects of palladium complexes on RAS-regulating proteolytic regulatory enzymes, which depend on the tumoral cell type. Figs. 8–10 show some of the most representative results. Thus, we have found that compounds $PdCl_2$(DANTU)·½CH_3OH (Fig. 8A) and $PdCl_2(PPh_3)_2$(DANU) (Fig. 8B) increase APA activity significantly in U373-MG cells, whereas compound $PdCl_2(PPh_3)_2$(MANU) (Fig. 8C) decreases this activity. No changes were found with other palladium complexes on APA activity in these cells (represented by Fig. 8D). On the contrary, none of the compounds significantly modified APA activity in NB69 cells (Fig. 8). On the other hand, all palladium complexes tested significantly increased APN in both NB69 and U373-MG cell types (Fig. 9 shows several examples from A to D). Finally, IRAP activity was differently modulated by palladium complexes depending on the tumoral cell type (Fig. 10). Thus, all tested complexes significantly decreased IRAP activity in U373-MG cells, whereas only complexes $PdCl_2(PPh_3)_2$(2MeOANU) (Fig. 10A), $PdCl_2(PPh_3)_2$(MVIO) (Fig. 10B) and $PdCl_2(PPh_3)_2$(DVIO)·CH_3OH (Fig. 10C) showed a significant inhibitory effect on IRAP activity in NB69 cells and depends on the complex concentration used. The remaining compounds showed a biphasic effect on IRAP activity in NB69 cells, where low concentrations showed an increase in IRAP activity and higher concentrations showed a decreased one (Fig. 10D). These results indicate that palladium complexes modify the proteolytic regulatory enzymes of RAS in a different way depending on the cell type, the catalytic route affected being also different. In any case, these changes modulate the bioactive efficacy of the different angiotensins, and therefore, of their functional roles as initiators/promoters of cell proliferation as autocrine/paracrine mediators.

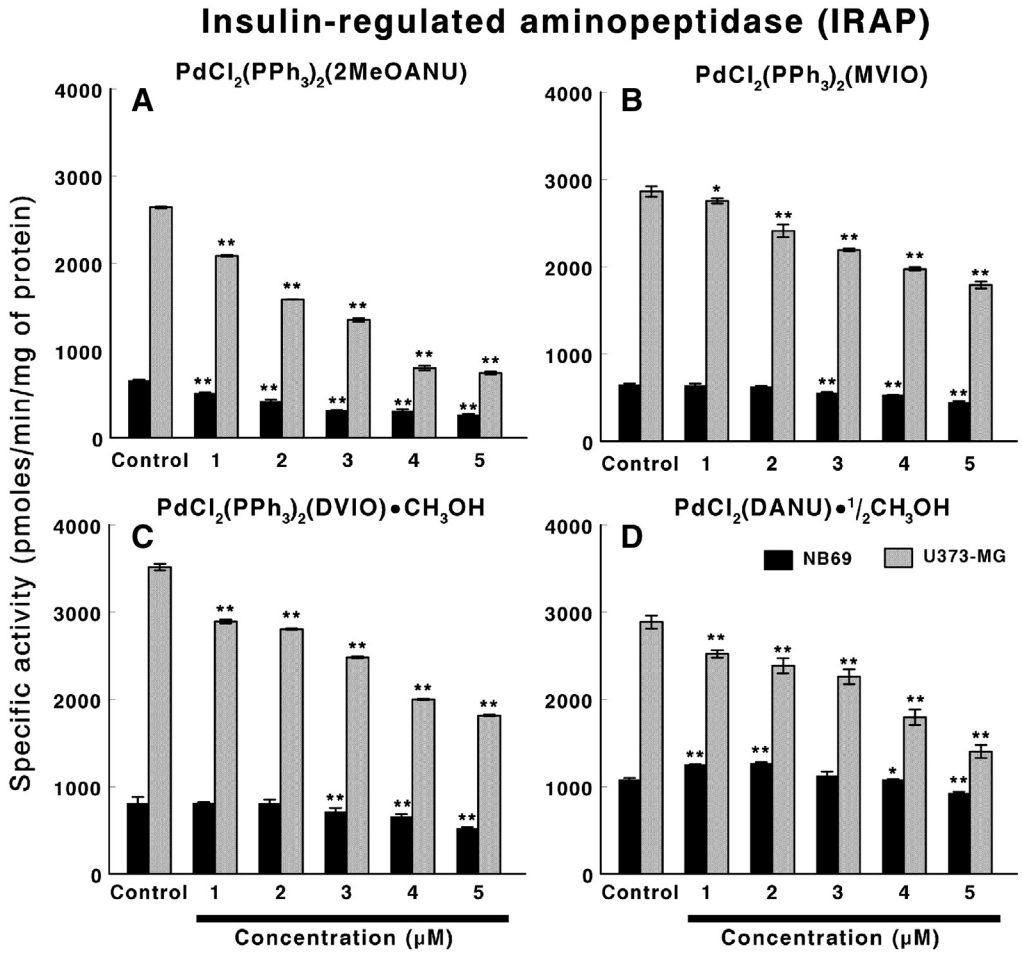

Fig. 10. Insulin-regulated aminopeptidase (IRAP) specific activity in human NB69 neuroblastoma and U373-MG glioma cell lines after the treatment with the palladium complexes **14** (A), **16** (B), **17** (C) and **3** (D). Results are expressed in pmol/min/mg of protein (Mean ± SEM; *P < 0.05; **P < 0.01; n = 4).

Also, other functions of the angiotensins not related to proliferation must be also modulated by palladium complexes.

Local tissue brain RAS is important in relationship with brain tumors because *in vivo* changes in RAS-regulating aminopeptidase activities in tumor tissue related to tumor growth in a model of glioma has been described. Thus, a time-dependent significant decrease in the specific activity of soluble and membrane-bound APN has been found, whereas the specific activity of soluble (but not membrane-bound) APA increased concomitantly with tumor growth [18]. In the RAS cascade, APA degrades AngII to form AngIII, and APN is the enzyme responsible for the degradation of AngIII to form AngIV [43]. These three bioactive peptides of the RAS, (AngII, AngIII and AngIV), exert their actions through their receptors AT_1, AT_2 and AT_4/IRAP [44,45]. These peptides play a local role in regulating cell differentiation and apoptosis [46] and other mechanisms not well known to date. Thus, it has been described that APA was up-regulated and enzymatically active in blood vessels of human tumors, but was not detected in normal blood vessels [47]. In addition, APA expression was found on dysplastic cells and was increased in precancerous lesions [48]. These data suggest that APA may play a regulatory role in neoplastic transformation and disease progression in cancer. On the other hand, other authors have reported that several kinds of carcinomas exhibited little expression of APN [49,50]. Although APN has been considered a proteolytic enzyme with the ability to facilitate tumor cell invasion through the extracellular matrix degradation [51], lower expression of APN implies that APN may enzymatically function in ways other than extracellular matrix degradation. Our data in experimental glioma *in vivo* suggests a predominant action of AngIII *vs.* AngII. The palladium complexes tested here differently modulate APN, APA and IRAP activities, which would induce changes in angiotensins bioavailability. This aspect is very interesting because it has been described that the amount of each angiotensin is not so important but the ratio between them which stimulates cell growth and angiogenesis [52]. Also supporting the importance of AngII/AngIII relationship, it has been described that selective blockage of one receptor could increase the effect of the other [47,53]. Therefore, the title palladium complexes show a putative specific antitumor activity against brain tumor cells.

Acknowledgments

Financial support of "Plan de Apoyo a la Investigación, al Desarrollo Tecnológico y a la Innovación" of the University of Jaén, PAIDI Junta de Andalucía (FQM273 and BIO296) is acknowledged.

Appendix A. Supplementary data

Tables with analytical and infrared data and renin–angiotensin system-regulating specific aminopeptidase activities in human neuroblastoma and glioma cell lines NB69 and U373-MG after the treatment with different palladium complexes and ligands are available. All atomic coordinates, anisotropic displacement parameters for non-hydrogen atoms and all interatomic distances and bond angles for compounds $[PdCl(DANUH_{-1})(CH_3CN)]\cdot\frac{1}{2}H_2O$ and $[PdCl(2MeOANUH_{-1})(CH_3CN)]$ have been deposited in the Cambridge Crystallographic Data Centre (CCDC numbers 871269 and 871271). These data can be obtained

free of charge *via* www.ccdc.cam.ac.uk/conts/retrieving.html; email: deposit@ccdc.cam.ac.uk.

References

[1] Y.Z. Liu, J. Vinje, C. Pacifico, G. Natile, E. Sletten, J. Am. Soc. 124 (2002) 12854–12862.
[2] J. Reedijk, Inorg. Chim. Acta 198 (1992) 873–881.
[3] R.W. Schrier, J. Clin. Invest. 110 (2002) 743–745.
[4] D. Kovala-Demertzi, A. Bocarelli, M.A. Demertzis, M. Coluccia, Chemotherapy 53 (2007) 148–152.
[5] A. Messere, E. Fabbri, M. Borgatti, R. Gambari, B.D. Blasio, C. Pedone, A. Romanelli, J. Inorg. Biochem. 101 (2007) 254–260.
[6] A.I. Matesanz, P. Souza, J. Inorg. Biochem. 101 (2007) 245–253.
[7] A.S. Abu-Surrah, K.A.A. Safieh, I.M. Ahmad, M.Y. Abdalla, M.T. Ayoub, A.K. Qaroush, A.M. Abu-Mahtheieh, Eur. J. Med. Chem. 45 (2010) 471–475.
[8] L. Yan, X. Wang, Y. Wang, Y. Zang, Y. Li, Z. Guo, J. Inorg. Biochem. 106 (2012) 46–51.
[9] A.S. Abu-Surrah, H.H. Al-Sádoni, M.Y. Abdalla, Cancer Ther. 6 (2008) 1.
[10] L. Tusek-Bozic, M. Juribasic, P. Traldi, V. Scarcia, A. Furlani, Polyhedron 27 (2008) 1317–1328.
[11] A. Garoufis, S.K. Hadjikakou, N. Hadjiliadis, Coord. Chem. Rev. 253 (2009) 1384–1397.
[12] S. Nadeem, M. Bolte, S. Ahmad, T. Fazeelat, S.A. Tirmizi, M.K. Rauf, S.A. Sattar, S. Siddiq, A. Hameed, S.Z. Haider, Inorg. Chim. Acta 363 (2010) 3261–3269.
[13] T.G. Spiro, Nucleic Acid–Metal Ion Interactions, John Wiley & Sons, New York, 1980.
[14] I. Votruba, A. Holy, K. Jost, FEBS Lett. 22 (1972) 287–288.
[15] N.A. Illán-Cabeza, A.R. García-García, M.N. Moreno-Carretero, J.M. Martínez-Martos, M.J. Ramírez-Expósito, J. Inorg. Biochem. 99 (2005) 1637–1645.
[16] J.M. Martínez-Martos, M. del Pilar Carrera-González, B. Duenas, M.D. Mayas, M.J. García, M.J. Ramírez-Expósito, Breast 20 (2011) 444–447.
[17] M.J. Ramírez-Expósito, M. del Pilar Carrera-González, M.D. Mayas, B. Duenas, J. Martínez-Ferrol, J.M. Martínez-Martos, Maturitas 72 (2012) 79–83.
[18] M.D. Mayas, M.J. Ramírez-Expósito, M.P. Carrera, M. Cobo, J.M. Martínez-Martos, Anticancer Res. 32 (2012) 3675–3682.
[19] F.A. Le Noble, J.W. Hekking, H.W. Van Straaten, D.W. Slaaf, H.A. Struyker Boudier, Eur. J. Pharmacol. 195 (1991) 305–306.
[20] Y. Marc, C. Llorens-Cortés, Prog. Neurobiol. 95 (2011) 89–103.
[21] R. Ardaillou, D. Chansel, Kidney Int. 52 (1997) 1458–1468.
[22] A.L. Albiston, S.G. McDowall, D. Matsacos, P. Sim, E. Clune, T. Mustafa, J. Lee, F.A. Mendelsohn, R.J. Simpson, L.M. Connolly, S.Y. Chai, J. Biol. Chem. 276 (2001) 48623–48626.
[23] S.Y. Chai, H.R. Yeatman, M.W. Parker, D.B. Ascher, P.E. Thompson, H.T. Mulvey, A.L. Albiston, BMC Neurosci. 9 (Suppl. 2) (2008) S14.
[24] G.M. Sheldrick, SADABS 2.10, 2003.
[25] G.M. Sheldrick, SHELXL-97, University of Göttingen, Germany, 1997.
[26] L.J. Farrugia, WINGX 1.70.01, University of Glasgow, Scotland, 2005.
[27] A.L. Spek, PLATON A Multipurpose Crystallographic Tool, Utrecht University, Utrecht, The Netherlands, 2003.
[28] Cambridge Crystallographic Data Centre MERCURY, 2002. (Cambridge, England).
[29] N.A. Illán-Cabeza, A.R. García-García, M.N. Moreno-Carretero, Inorg. Chim. Acta 366 (2011) 262–267.
[30] W.J. Geary, Coord. Chem. Rev. 7 (1971) 81–122.
[31] J.N. Low, R.A. Howie, F. Hueso Ureña, M.N. Moreno Carretero, Acta Crystallogr. C48 (1992) 145–147.
[32] J.N. Low, S.N. Scrimgeour, C. Egglishaw, R.A. Howie, F. Hueso Ureña, M.N. Moreno Carretero, Acta Crystallogr. C50 (1994) 1329–1333.
[33] J.M. Salas, M.A. Romero, M.P. Sánchez, M.N. Moreno, M. Quirós, J. Molina, R. Faure, Polyhedron 17 (1992) 2217–2222.
[34] G. Ferguson, J.N. Low, M. Quirós Olozabal, J.M. Salas Peregrín, F. Hueso Ureña, M.N. Moreno Carretero, Polyhedron 19 (1996) 3233–3239.
[35] C. Janiak, J. Chem. Soc. Dalton Trans. (2000) 3885–3896.
[36] D. Lin-Vien, N.B. Colthup, W.G. Fateley, J.G. Grasselli, The Handbook of Infrared and Raman Characteristic Frequencies of Organic Molecules, Academic Press, Boston, 1991.
[37] N.A. Illán-Cabeza, A.R. García-García, M.N. Moreno-Carretero, Comput. Theor. Chem. 964 (2011) 83–90.
[38] G. Cruz Bermúdez, A. García Rodriguez, M.N. Moreno Carretero, J.M. Salas Peregrín, C. Valenzuela Calahorro, Monatsh. Chem. 118 (1987) 329–335.
[39] B.R. Singh, S.C. Ojha, R. Ghosh, Thermochim. Acta 101 (1986) 359–364.
[40] M.A. Romero, J.M. Salas, M. Simard, M. Quirós, A.L. Beauchamp, Polyhedron 9 (1990) 2733–2739.
[41] K. Nakamoto, Infrared and Raman Spectra of Inorganic and Coordination Compounds, 5th ed. Wiley & Sons, New York, 1997.
[42] J.R. Ferraro, Low-frequency Vibrations of Inorganic and Coordination Compounds, Plenum Press, New York, 1971.
[43] A.J. Barrett, N.D. Rawlings, J.F. Woessner, Handbook of Proteolytic Enzymes, 2nd ed. Elsevier Academic Press, Amsterdam, Boston, MA, 2004.
[44] Y. Kambayashi, S. Bardhan, K. Takahashi, S. Tsuzuki, H. Inui, T. Hamakubo, T. Inagami, J. Biol. Chem. 268 (1993) 24543–24546.
[45] M. Mukoyama, M. Nakajima, M. Horiuchi, H. Sasamura, R.E. Pratt, V.J. Dzau, J. Biol. Chem. 268 (1993) 24539–24542.
[46] E. Escobar, T.S. Rodríguez-Reyna, O. Arrieta, J. Sotelo, Curr. Vasc. Pharmacol. 2 (2004) 385–399.
[47] O. Arrieta, B. Pineda-Olvera, P. Guevara-Salazar, N. Hernández-Pedro, D. Morales-Espinosa, T.L. Cerón-Lizarraga, C.H. González-De la Rosa, D. Rembao, B. Segura-Pacheco, J. Sotelo, Br. J. Cancer 99 (2008) 160–166.
[48] H. Fujimura, K. Ino, T. Nagasaka, N. Nakashima, H. Nakazato, F. Kikkawa, S. Mizutani, Oncology 58 (2000) 342–352.
[49] J. Dixon, L. Kaklamanis, H. Turley, I.D. Hickson, R.D. Leek, A.L. Harris, K.C. Gatter, J. Clin. Pathol. 47 (1994) 43–47.
[50] A. Varona, L. Blanco, J.I. Lopez, J. Gil, E. Agirregoitia, J. Irazusta, G. Larrinaga, Am. J. Physiol. 292 (2007) F780–F788.
[51] I. Saiki, H. Fujii, J. Yoneda, F. Abe, M. Nakajima, T. Tsuruo, I. Azuma, Int. J. Cancer 54 (1993) 137–143.
[52] J. Teranishi, H. Ishiguro, K. Hoshino, K. Noguchi, Y. Kubota, H. Uemura, Prostate 68 (2008) 1666–1673.
[53] O. Arrieta, P. Guevara, E. Escobar, R. Garcia-Navarrete, B. Pineda, J. Sotelo, Br. J. Cancer 92 (2005) 1247–1252.